Validation of Recent Improvements in Phast Dispersion Modelling

Frank Hart and Mike Harper, DNV Digital Solutions, Applicon House, Stockport, SK3 0EY

The Unified Dispersion Model (UDM) is a key component in the Phast and Safeti consequence and risk modelling packages. It models the dispersion of accidental releases to the atmosphere and its validation underpins confidence in analysis of hazards. This paper will present recent improvements to the UDM together with their validation against experimental data. This work has focused on the following areas:

Heavy gas spreading. The breakdown of gravity spreading for heavy gas clouds can occur once vertical concentration gradients become eroded, and we have included a simple model describing this process in the UDM. Its adoption improves prediction of cloud width and dispersion distances for the recently published Jack Rabbit 2 chlorine trials, and we present new validation results illustrating this.

Buoyant gas dispersion. Increasingly the consequences of hydrogen releases have become an area of interest. Two-phase releases while initially heavier than air will subsequently evaporate and become buoyant. Recent work has improved the modelling in such scenarios, including allowing lift-off from the ground. While experimental data is scarce, we have been able to undertake some qualitative comparisons which demonstrate the advantages of the new modelling.

Modelling of vertical or angled releases. New and modified crosswind entrainment correlations have significantly improved near-field predictions of concentration and trajectory for relatively low-velocity stack-type releases. Validation has been carried out against a large data set of wind-tunnel experiments and some field-scale releases.

All the model improvements described have been included as default options from Phast 8.61, and the validation runs are available from DNV as standard sets of Phast study files. Running these studies generates results immediately comparable to published experimental data points. The intention is to make our assumptions, model inputs and results transparent for Phast users.

Keywords: dispersion, validation, consequence modelling,

Introduction

Accurate estimation of hazards from loss of containment events requires robust consequence modelling that can cope with a range of release scenarios and materials. In particular atmospheric dispersion modelling is the basis of many hazard calculations for flammable (LFL distances, explosions) and toxic (threshold concentrations or probits) materials. Confidence in these models is primarily underpinned by validation studies, where the results of field, wind-tunnel or lab-scale experiments are compared with model predictions.

A very wide range of plausible dispersion scenarios can be considered: these can vary in terms of time-dependency, thermodynamics, momentum, buoyancy, environment, and geometry. Some of these are poorly represented in published datasets and validation may be limited or absent. There is a drive to continually extend and improve model validation in response to newly available data, regulatory requirements, emerging processes or materials.

The dispersion model in Phast and Safeti is the Unified Dispersion Model (Witlox & Holt, 1999). It comprises linked sub-models for jet, heavy gas and passive dispersion along with a thermodynamic model to calculate phase distribution and cloud temperatures, and an integrated rainout and pool re-evaporation model.

The UDM has an extensive published history of validation (Witlox, et al., 2018). This paper presents more recent model improvements and subsequent validation in the UDM to bring this work up to date for the Phast 8.61 release. The work covers ~~four~~ three aspects which are discussed separately in subsequent sections:

1. Heavy gas spreading.
2. Buoyant lift-off.
3. Vertical or angled releases.

Heavy gas spreading

Background and model implementation

The Jack Rabbit II field trials (Fox, et al., 2022) in 2015 and 2016 in Nevada released large amounts of pressurised liquid chlorine through large diameter orifices in a range of orientations. The programme included comparing observed concentrations and cloud widths against a range of models, including the UDM (Mazzola, et al., 2021) . Three experiments were considered: Trials 1, 6 and 7. The first two were vertically impinging releases from the bottom of the tank; the latter was angled down at 45°. It was clear that in the far-field concentrations were underestimated, and widths significantly over-estimated.

The cloud predicted by the UDM was dominated by heavy gas spreading. This regime is assumed to end only when the cloud meets the criteria for the transition to passive spreading and entrainment. However, there is evidence that gravity spreading can be effectively shut down much earlier than this. The experiments of Linden and Simpson (1988) demonstrated turbulence can destroy cloud vertical stratification and significantly reduce spread rates. A model derived from these experiments stipulates reduced spread rates, as well as a transition criterion. This was adopted by HEGADAS (Post & others, 1994) and performed well against the HTAG experiments of Peterson and Ratcliff (1989).

For this work we adapted this "gravity spreading collapse" (GSC) model for the UDM. It compares the volume of top air entrainment to the volume added by crosswind spreading. If the former exceeds the latter, we assume the increasing height of the cloud disrupts the well-defined flows associated with the gravity current resulting in a much-reduced spread rate. Specifically, the point of collapse is defined as a transition point when

$$\frac{W_{eff}}{H_{eff}}\frac{u_e}{u_g} \geq 1 \tag{1}$$

W_{eff} and H_{eff} are respectively the cloud effective width and height, u_e is the top-entrainment velocity, and u_g the lateral spread velocity. For the new model to be considered, the cloud must be sufficiently heavy ($Ri_* > 35$), and past the point of rainout and not over a pool (where the ratio W_{eff}/H_{eff} is large but not due to gravity spreading). Moreover, we require a strong gravity flow to have been established: the above condition must be continuously satisfied for a characteristic spreading time t_g calculated from when the condition is first met:

$$t_g = \frac{W_{eff}}{u_g} \tag{2}$$

This will prevent for example only very transiently dense clouds from LNG spills from triggering this behaviour. The reduced post-transition spread rate is given by

$$\frac{dW_{eff}}{dt} = \frac{u_* Ri\ \Phi(Ri_*)}{3\kappa C}\frac{H_{eff}}{W_{eff}} \tag{3}$$

Here u_* is the friction velocity, Ri the Richardson number, Φ the Richardson function, κ the Von Karman constant and C an empirical constant for which we assume to be the same as HEGADAS ($C = 5$). The HEGADAS documentation points out weaknesses in the post-transition spreading rate in that it has incorrect asymptotic behaviour in the far-field. We anticipate most cases will transition to passive modelling before this becomes a problem.

Source terms

We have compared experimental results against the latest Phast release (8.61) for the three Jack Rabbit II trials 1, 6 and 7. The release was not modelled as a liquid as Phast will overpredict pool rainout for an impinging release. Instead, Table 3 in Mazzola et al. describes a two-segment source term (primary release – rainout, and evaporative pool source). However, a discontinuous source term in the UDM can cause model artifacts and for this work we have used a single continuous segment with the mass rate and velocity from the modified primary release, and duration extended such that overall mass released is conserved. This assumption also allows use of the quasi-instantaneous model (QI) which allows continuous releases to transition to instantaneous clouds when cloud width significantly exceeds length. The Jack Rabbit releases are short-duration relative to the medium and far field dispersion times, and representing the cloud as being instantaneous has some merit in these terms. Temperatures were adjusted slightly up ($<$ 0.2 ℃) to ensure a vapour release.

Case	Trial 1	Trial 6	Trial 7	Notes
Mass rate (kg s^{-1})	188.2	202	196	Primary release – rainout
Duration (s)	24.16	41.4	44	Extended to conserve mass
Velocity (m s^{-1})	50.8	44.2	44.2	
Temperature (°C)	-37.2	-37.2	-37.2	Adjusted slightly to ensure vapour
Orientation (° below horizontal)	90	90	45	'Impinged' option not used
Windspeed (m s^{-1} at 2m) / Stability	1.45 / F	2.42 / E	3.98 / D	Trial 7 was given as D or E, Trial 1 as E or F

Table 1. Source terms and key inputs used in this work

Results and Discussion

Results are given with and without the GSC model, and for the QI model. Figure 1 plots observed against predicted results for arcwise maximum concentrations and the geometric mean bias for the predictions.

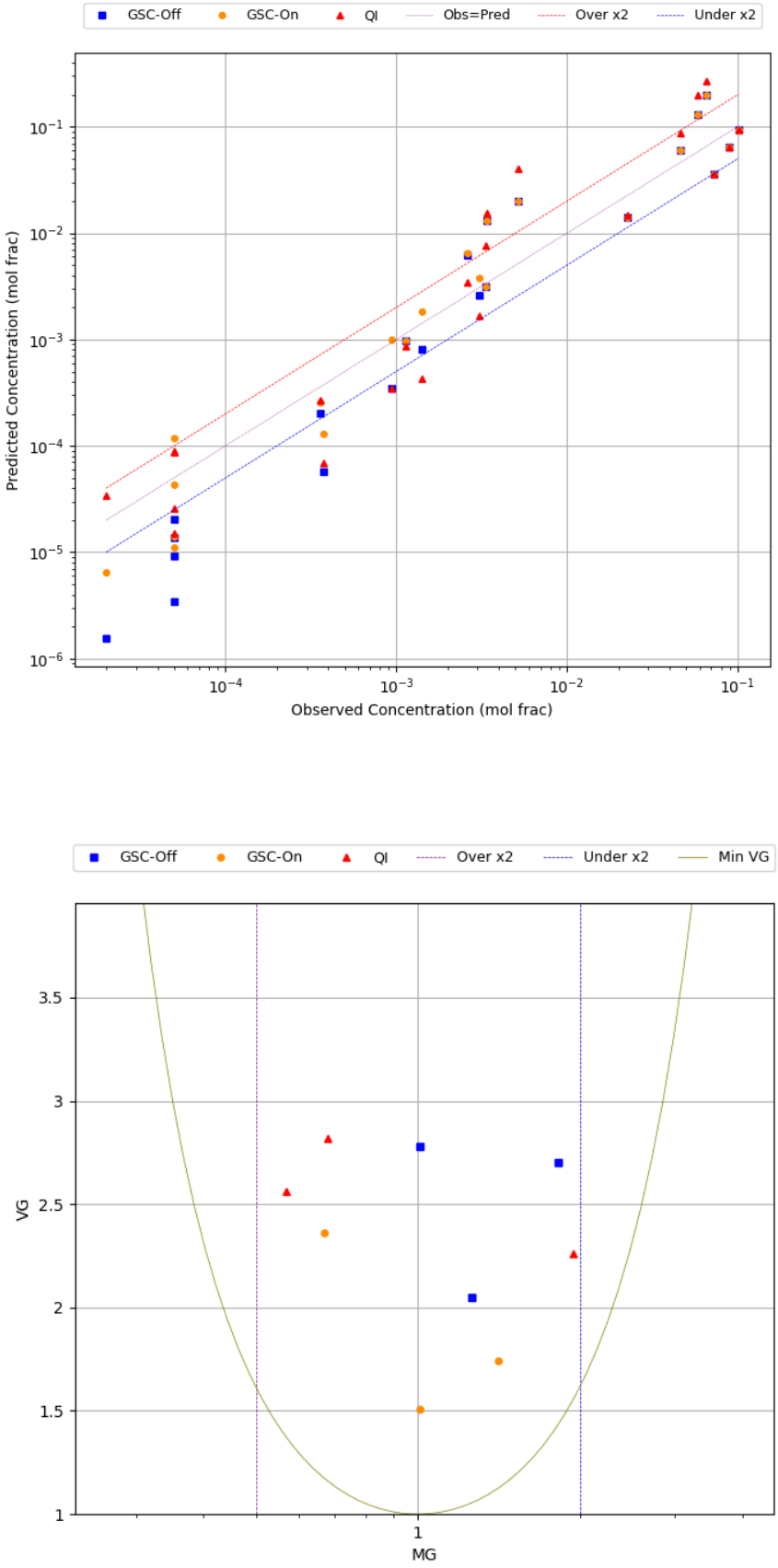

Figure 1: Observed vs predicted maximum arcwise concentrations (top) and geometric mean bias (bottom) for Jack Rabbit Trials 1, 6 and 7: GSC off, GSC on and QI

Both GSC and QI give significantly improved results over the previously reported results. The bias towards underestimating arc wise concentrations in the far-field is largely removed. QI is a little conservative on concentrations but is the best by far for cloud width. It is worth noting for Trial 1, the releases were within an array of shipping containers which cannot be represented by Phast.

The GSC widths are still too large however, despite being much reduced by adopting GSC. Our results for GSC on and off suggests that the default Phast approach of modelling this using a steady-state simulation may inherently over-predict lateral spreading, despite a post-processed correction for along-wind spreading. Further work in this area is planned.

Other experiments affected by this change include Thorney Island continuous releases (McQuaid & Roebuck, 1985) and Goldfish (Blewitt, et al., 1987). These (in particular Goldfish) show a significant improvement over results without GSC.

Buoyant gas spreading and lift-off

Buoyant gases such as methane, hydrogen or ammonia are often stored as liquids either below their boiling point or in pressurised form. When released these will flash but may still contain large liquid fractions causing the cloud to be denser than air. They can therefore transition to the heavy spreading regime in the UDM but, once the liquid rains out or evaporates they will become buoyant. There are two significant limitations in earlier Phast versions when this happens that have been overcome in the most recent version of the model.

Spreading

The cloud spread rate in the heavy gas regime is proportional to the square root of the density difference between cloud and air density:

$$\left.\frac{dW_{eff}}{dt}\right|_{hvy} \propto \sqrt{max(0, \rho_{cld} - \rho_a)} \tag{4}$$

For buoyant clouds this evaluates to zero. Any entrainment of air into the cloud therefore is constrained to make the cloud taller rather than wider. Once the cloud goes passive this constraint ends, but if this is significantly delayed (as it can be for a very buoyant cloud) then an unrealistic cloud geometry can have developed. To correct this, we have adopted in the heavy gas phase the spread rate to be the maximum of near-field, heavy and passive spread rates to ensure a realistic minimum lateral spread.

$$\frac{dW_{eff}}{dt} = max\left[\left.\frac{dW_{eff}}{dt}\right|_{nf}, \left.\frac{dW_{eff}}{dt}\right|_{hvy}, \left.\frac{dW_{eff}}{dt}\right|_{pass}\right] \tag{5}$$

Lift-off

In earlier Phast versions, clouds that have become heavy cannot thereafter lift off. For materials such as LNG – and especially for liquid hydrogen – this may produce over-conservative ground level concentrations. In other situations, a modified version of the Briggs criterion (Briggs, 1984) is applied

$$Ri_* = \frac{g[\rho_{cld} - \rho_a(z = z_{cld})]H_{eff}}{\rho_a {u_*}^2} < -20 \tag{6}$$

Enabling lift-off in all cases however based on an instantaneous evaluation of the criterion using local density can mean that clouds that are only transiently buoyant may lift off. For this reason, we have added in a requirement that for lift-off the requirement must be continuously satisfied for a time t_{lo}. This we determine by taking an appropriate length scale, L, for the cloud, and determining from the acceleration due to buoyancy how much time would be required for the cloud to ascend that high (i.e. effectively become detached from the ground)

$$L = \frac{\sqrt{W_{eff} H_{eff}}}{2} \tag{7}$$

$$t_{lo} = \sqrt{\frac{2L}{g\,(\rho_a - \rho_{cld})/\rho_a}} \tag{8}$$

It can be argued that a better value for L would be H_{eff}. However, this would result in very flat clouds lifting off too easily. In practice one would expect lift off to be associated with a vertical stretching of the cloud.

Comparison with experiments

The experiments of Witcofski and Chirivella (1984) involved spilling 5.7m^3 of liquid hydrogen onto the ground and measuring concentrations at various distances and heights downwind. The release durations and therefore rates varied. There is limited data presented in the paper – principally for Test 6. The key inputs are release rate = 11.5 kg s^{-1}, duration = 35s, elevation = 1m, weather 2.2/D, atmospheric temperature = 15°C, relative humidity = 29%. The experimental results were digitised from Figure 7 in that paper. They are not time-averaged, and significant fluctuations occur over timescales of seconds.

Formal verification is therefore not possible but as an illustration of the changes we can compare a snapshot of results with Phast (Figure 2). The Phast 8.4 results suffer from both the problems described above: the cloud does not lift-off, and crosswind spreading becomes zero meaning the cloud grows too tall. Although somewhat larger than the actual plume, Phast 8.61 exhibits lift-off at around the same point. In addition (although the images are not reproduced here) qualitatively the Phast simulations for version 8.61 capture the behaviour observed in their photographs Figures 10 and 11.

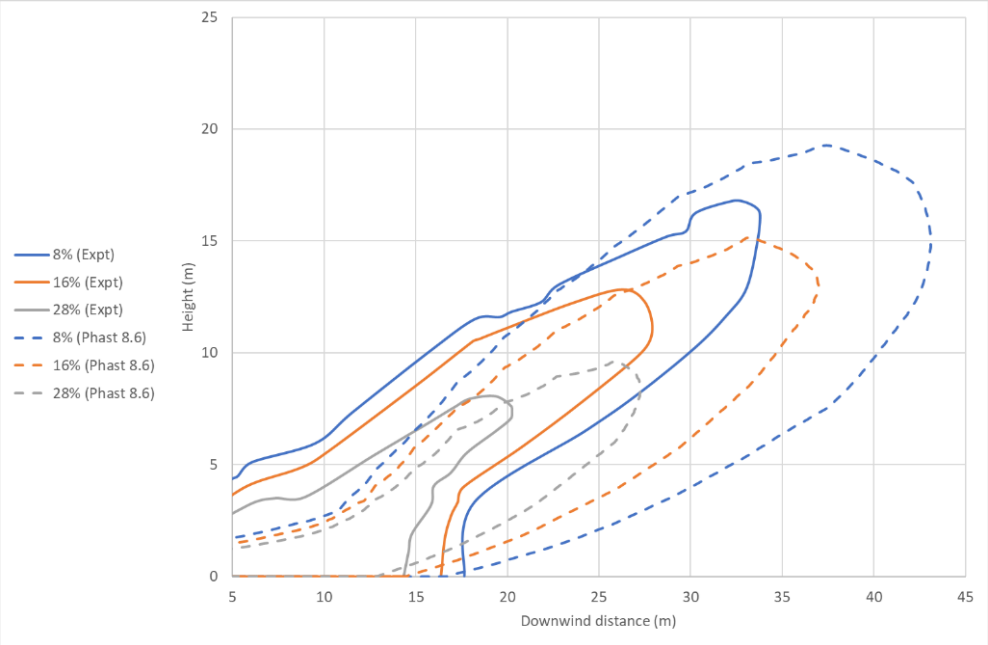

Figure 2: Lift-off of liquid hydrogen spill - sideview at ~21 secs. Case 6 (Figure 7) from Witcofski and Chirivella

Modelling of vertical/angled releases

A common application area for the UDM is for angled or vertical releases, such as modelling emissions from industrial chimney stacks. In such cases, and indeed for dense horizontal releases which are exposed to a crosswind as they follow a downwards trajectory, the UDM models increased air entrainment into the plume due to the crosswind impact of wind on the plume.

It became apparent that such releases may result in ~~be~~ under-predicted concentrations in Phast. This conclusion was based on a set of predominantly wind tunnel experiments for gas released vertically or angled into a cross flow (Donat & Schatzmann, 1999; Quillatre, 2017; Schatzmann, et al., 1993; Vidali, et al., 2019). Details of these experiments, with wind tunnel experiments modelled at field scale rather than wind tunnel scale, are summarised in Table 2.

Experiment	Release Height (m)	Diameter (m)	Release Velocity (m s^{-1})	Release Angle (°)	Density (kg m^{-3})	Wind Velocity (m s^{-1})	Surface Roughness (m)	Velocity Ratio *R*
Schatzmann 4T	5.0	0.159	603	90	2.00	20.3	0.037	33.0
Schatzmann 10T	8.5	1.27	16.5	90	2.77	6.7	0.037	2.54
Schatzmann 11T	8.5	1.27	16.5	90	2.77	13.3	0.037	1.27
Schatzmann 15T	8.5	1.27	28.5	90	5.88	11.5	0.037	2.54
Donat 1	7.0	0.58	43.8	90	1.88	8.9	0.008	5.2
Donat 3	6.7	1.0	14.7	90	2.77	12.3	0.008	1.27
Donat 4	6.7	1.0	14.7	90	2.77	12.9	0.19	1.27
Donat 5	6.7	1.0	25.3	90	5.88	10.7	0.08	2.54
Donat 10	15.0	0.8	28.5	45	2.77	10.1	0.07	2.0
Donat 11	15.0	0.8	21.1	90	2.77	10.1	0.07	2.0
Donat 19	9.0	0.3	174	0	2.77	11.3	0.07	14.8
Donat 21	9.0	0.3	163	90	2.77	11.3	0.07	14.8
Donat 44	8.7	0.58	67.3	0	2.77	13.8	0.008	4.0
Vidali	7.6	1.2	22.9	90	1.74	14.2	0.011	2.6
Quillatre H6	5.65	0.152	22.6	0	1.38	1.4	0.01	15.4
Quillatre V6	4.65	0.152	16.2	90	1.38	2.2	0.01	8.1
Quillatre V18	4.45	0.457	4.5	90	1.38	4.2	0.01	0.95

Table 2. Experimental data set used for validation of crosswind releases

We have modelled these releases in Phast (using the 8.4 default settings) and the initial Phast validation of centreline concentrations are shown using the blue markers in and Figure 3 (a) and (b). The plot of observed against predicted concentrations Figure 3 (a) confirms a consistent trend for Phast to under-predict. This is trend is evident in the geometric mean bias plot in Figure 3 (b) where almost all experiments appear on the right of the plot. Validation of vertical releases within Phast has historically been focussed on trajectory (Pratte & Baines, 1967; Briggs, 1984) rather than concentration, but the concentration results here ~~.~~ suggest the degree air entrainment predicted by Phast for this type of release is too large.

Existing Models

A jet released at an angle into a horizontal air stream is often modelled as experiencing increased air entrainment, and/or an additional horizontal momentum. The UDM has historically used the Morton model (Morton, et al., 1956) which assumes for continuous releases the crosswind entrainment E_{cross} (kg m^{-1} s^{-1}) is given by

$$E_{cross} = \alpha_2 \rho_a P_{above} |u_a sin\theta| \quad (9)$$

The air drag on a plume in the UDM is given by:

$$F_{drag} = C_d \rho_a P_{above} (u_a sin\theta)^2 \quad (10)$$

By default in Phast 8.4, $C_d = 0$ and no modification is applied to cloud momentum. Any effect on the cloud trajectory is assumed to derive from additional entrainment of air with horizontal momentum. As shown, this model has a clear bias towards under-predicting maximum (centreline) concentrations, and a review of relevant studies was completed to understand its deficiencies.

A jet released into a cross flow has many industrial applications and as such has been the subject of many studies. These types of flow are often characterised by the velocity ratio R, which can be generally defined for angled releases as

$$R = \frac{u_s - u_a(h_s)\cos\theta}{u_a(h_s)} \quad (11)$$

where u_s is the source exit velocity and $u_a(h_s)$ is the ambient velocity at the release height h_s. For vertical releases this reduces to the ratio of exit velocity to ambient velocity at release height.

The literature provides a wide range of work on jets emerging into a cross flow, such as the experimental studies of Kamotani & Greber (1972) and the detailed numerical simulations of Yuan & Street (1998) and Muppidi & Mahesh (2008). These studies and those of other workers indicate a complex interaction between the jet and the cross wind, particularly in the early stages of the trajectory. The common features emerging from the literature which are of particular interest to the problem at hand are:

- suppression of near-field crosswind entrainment, with observed entrainment similar to that of a free jet; and
- presence of a near-field drag effect acting across the jet.

Ooms (1972) proposed a model with these desired properties, which is similar to the Morton model but with an additional $\cos\theta$ term which has the effect of suppressing entrainment when the cloud is vertical or near vertical:

$$E_{cross} = \alpha_2 \rho_a u_a (2\pi b)|\sin\theta|\cos\theta \tag{12}$$

An E_{cross} entrainment coefficient of $\alpha_2 = 0.43$ and a drag coefficient in the F_{drag} expression (Eq. 10) of $C_d = 0.13$ is recommended (when converted to the UDM formulation). Hence it appears to address the two features identified above. We have implemented this model in Phast since version 8.4, but it does not improve performance significantly for the experimental data set.

An alternative model has therefore been developed to account for these effects, which is outlined in the next section.

Extended Model

Based on the performance of the Morton and Ooms models, an extension to the Morton model was developed targeted specifically at the relatively low velocity angled and vertical releases covered in the experimental test set.

Entrainment

The approach taken is similar to that used by Cleaver & Edwards (1990) with an initial region of zero crosswind entrainment followed by a region of partial suppression where entrainment is phased in linearly over distance. We define a reduced entrainment term E'_{cross} as

$$E'_{cross} = \begin{cases} 0 & s \le L_{core} \\ \left(\dfrac{s - L_{core}}{L_{supp} - L_{core}}\right) E_{cross} & L_{core} < s \le L_{supp} \end{cases} \tag{13}$$

The transitionary part of the flow immediately beyond the point of emergence (the potential core) represents a region where the properties on the centreline of the jet remains unaffected by the crossflow. For angled and vertical releases Kamotani & Greber (1971) define L_{core} as a function of diameter D and velocity ratio R

$$L_{core} = \frac{6.4D}{1 + (4.6/R)} \tag{14}$$

Beyond this region, there is a subsequent suppression distance (L_{supp}) where the crosswind entrainment increases rapidly from zero. The extent of this region is difficult to bound and the dependence on density and velocity ratio unclear, but the studies of Kamatoni & Greber and Yuan & Street show broadly linear mass & volume flux relationships beyond 8-12D in their studies. To align with this, we have calculated this region as a multiple of L_{core} :

$$L_{supp} = \left(1 + \sqrt{\frac{\rho_0}{\rho_a}}\right) L_{core} \tag{15}$$

At trajectory distances beyond L_{supp}, the crosswind entrainment is as per the Morton model.

Crosswind Drag

The application of a crosswind drag force has been introduced into the model but is also restricted to the near trajectory. This can be considered as ‘solid body’-like effect where emerging jet retains a high degree of integrity, presenting a relatively well-defined obstacle to the cross flow thereby forcing the flow to separate and pass around. As entrainment increases and the plume loses this integrity, the crosswind can increasingly intrude directly and so the drag effect correspondingly reduces.

The UDM already accommodates a drag term acting perpendicular to the jet axis, although typically the drag coefficient $C_d = 0$ is used. This functionality has been used represent the desired short-lived drag effect by using a variable drag coefficient, which is phased out over a trajectory distance. As entrainment suppression and drag can be considered related (drag strongest where crosswind entrainment suppressed and vice-versa), the phase-out length L_{drag} of the drag coefficient is taken to be a simple multiple of the suppression distance. While not overly sensitive to this value, a multiple of three times the suppression distance has been used to account for the long tail to the effect reported by Mahesh (2013). The update to the UDM has therefore been to allow the linear reduction of the drag coefficient from its initial value to zero over L_{drag} over the trajectory length s

$$C_d = C_{drag}^{init}\left(1 - \max\left[\frac{s}{L_{drag}}, 1\right]\right) \qquad L_{drag} = 3L_{supp} \tag{16}$$

The initial value of drag coefficient remains a configurable parameter in the model, with a default value of $C_d^{init} = 0.39$ used, three times the Ooms drag coefficient (in UDM terms). A full optimisation of this parameter has not been undertaken

but based on a few selected values provides the best choice across the validation set considered. It also aligns with the Yuan & Street suggestion (1998) that the drag coefficient is initially higher than might be expected for a cylindrical obstruction because of the concave distortion of the jet on the downwind side.

Validation & Discussion

Figure 3 (a) and (b) shows the initial and updated Phast validation of centreline concentration for the 17 experiments. The plot of observed against predicted concentrations in Figure 3 (a) shows the consistent trend for Phast to under-predict - especially in the near-field - is removed, with many predictions now appearing above the observed line with the Morton Extended model (orange markers). This is also illustrated in the geometric mean bias plot in Figure 3 (b) where the experiments are more evenly scattered around MG=1 with the Morton Extended model rather than consistently appearing on the right of the plot.

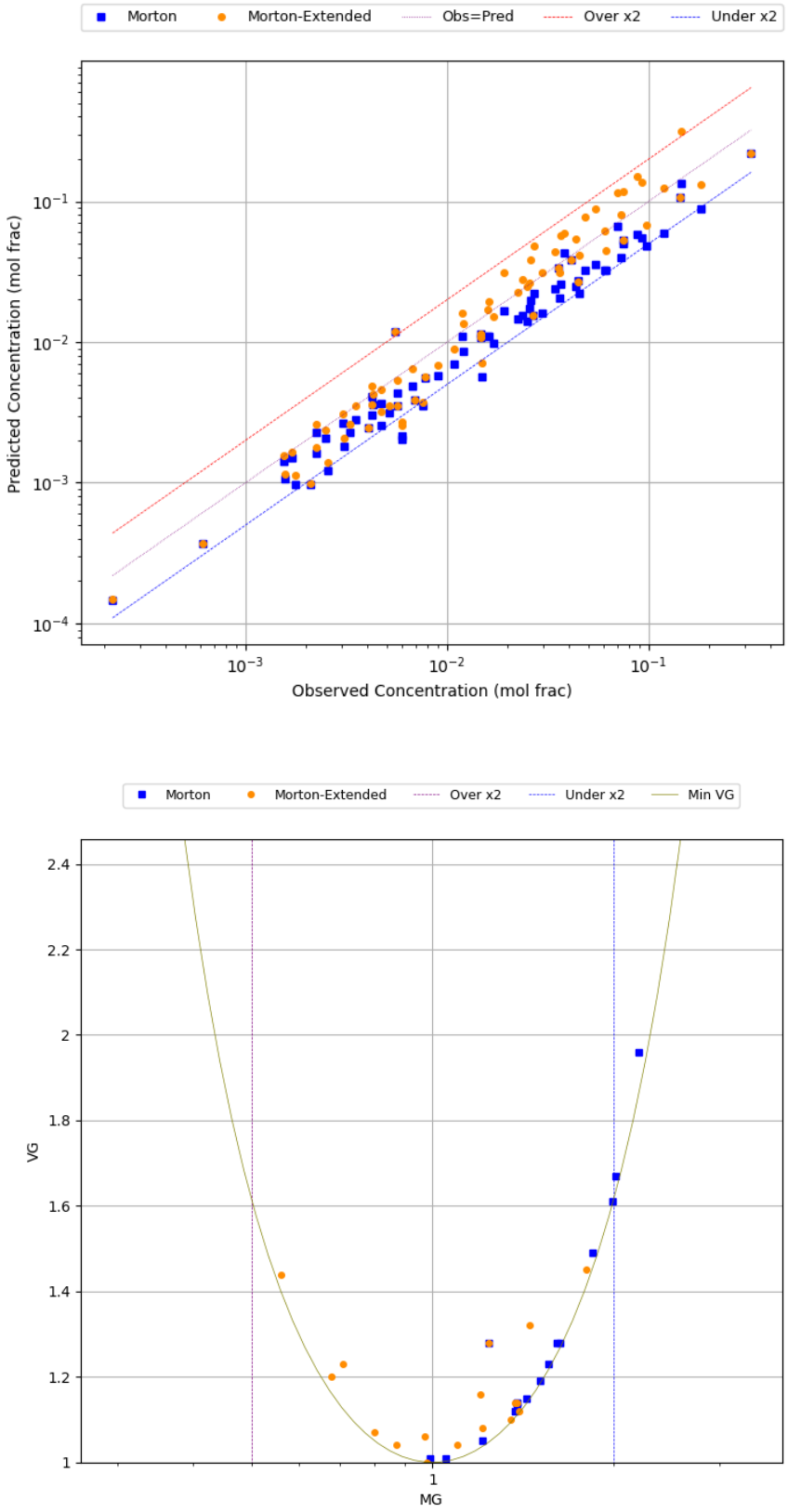

Figure 3: Validation of Morton (blue markers) and Morton extended (orange markers) model predictions of crosswind experiments: (a) observed vs predicted centreline concentrations (upper); and (b) geometric mean bias (lower)

Overall, the Morton Extended model is a significant improvement in concentration predictions for low R vertical or angled releases and has been the default jet model in Phast since 8.6. The main sources of literature and validation data for this type of release are in relation to low velocity releases, so the work presented here is necessarily focussed in this area, and indeed aligns with the main application areas anticipated such as industrial stack and vent emissions. The validation set against which the models have been assessed have a maximum $R = 33$, but most experiments have $R < 10$. We can therefore have a high degree of confidence in the application of this model to releases with R in this range.

Due to the limitations on the experimental data, the extended model is deliberately formulated to not significantly change predictions where $R \gg 20$. Such releases are expected to behave like free jets for longer so we might expect resistance to crosswind entrainment and also the presence of a crosswind drag effect to persist over a correspondingly longer distance. Work is progressing in this area and extension into the high R range expected in a future Phast release.

Summary and Conclusions

The modifications to the UDM discussed in the previous sections are generally limited in scope and improve outcomes for several specific scenarios or types of release. These include liquid spills of buoyant gases (e.g., LH2), large dense-gas releases (e.g. CO_2), or low-velocity stack releases. More generally results will be very similar to those in previous versions. In undertaking this work, we have significantly both improved the performance of the UDM against experiments and extended the scope of that validation. It has suggested items of further work where there is a lack of field-scale experimental data, for example high velocity vertical releases or spills of buoyant gases.

All the Phast 8.61 cases to reproduce the results are available from DNV.

Acknowledgements

The authors would like to thank Derek Miller and Beth Lutostansky from Air Products for bringing our attention to weaknesses in modelling low velocity vertical releases, and Elena Vyazmina from Air Liquide for collating experimental data on the same.

Glossary

α_2	Crosswind entrainment coefficient
b	The characteristic half-width of the plume in the Ooms crosswind entrainment model, m
C_d	Drag coefficient
D	Source diameter, m
E_{cross}	Crosswind entrainment rate, $kg\ m^{-1}\ s^{-1}$
F_{drag}	Plume drag force, $N\ m^{-1}$
GSC	Gravity spreading collapse. Transition to a lower lateral spreading rate within the heavy gas model
H_{eff}	Effective half-height of the UDM plume, m
h_s	Source release height, m
HEGADAS	Heavy gas dispersion model in the HG System suite of dispersion models
κ	Von Karman constant
L_{core}	Length of the potential core, where centreline concentration is unaffected by the cross flow, m
L_{supp}	Length of the region where crosswind entrainment is suppressed, m
L_{drag}	Length of the region where a drag force is applied to the plume, m
P_{above}	Above-ground perimeter of the cloud, m
$\Phi(Ri)$	Entrainment function used in the UDM to calculate entrainment rates in a heavy cloud
QI	Quasi-instantaneous. A short-duration cloud is replaced by an equivalent instantaneous one
R	Ratio of source gas velocity to crosswind velocity
Ri/Ri_*	Richardson number
ρ_a	Ambient air density, $kg\ m^{-3}$
ρ_0	Plume density at the release source, $kg\ m^{-3}$

ρ_{cld}	Plume density at location of interest, $kg\ m^{-3}$
t_g	Characteristic time for a plume to display heavy gas properties before the GSC transition is allowed, s
t_{lo}	Characteristic time for which the Briggs criterion must be satisfied before lift-off is allowed, s
u_e	Top entrainment velocity of a heavy gas cloud, $m\ s^{-1}$
u_g	Lateral spreading velocity of a heavy gas cloud (dW_{eff}/dt), $m\ s^{-1}$
u_s	Source release velocity, $m\ s^{-1}$
u_*	Friction velocity, $m\ s^{-1}$
u_a	Windspeed, $m\ s^{-1}$
UDM	Unified dispersion model, the dispersion model used within Phast
W_{eff}	Effective half-width of the UDM plume, m
z_{cld}	Height above the ground of the plume centre line, m

References

Blewitt, D. N., Yohn, J. F., Koopman, R. P. & Brown, T. C., 1987. *Conduct of anhydrous hydrofluoric acid spill experiments.* s.l., s.n., p. 2–4.

Briggs, G. A., 1984. Plume rise and buoyancy effects. *Atmospheric science and power production*, Volume 850, p. 327–366.

Cleaver, R. P. & Edwards, P. D., 1990. Comparison of an integral model for predicting the dispersion of a turbulent jet in a crossflow with experimental data. *Journal of Loss Prevention in the Process Industries*, 1, Volume 3, p. 91–96.

Donat, J. & Schatzmann, M., 1999. Wind tunnel experiments of single-phase heavy gas jets released under various angles into turbulent cross flows. *Journal of Wind Engineering and Industrial Aerodynamics*, November, Volume 83, p. 361–370.

Fox, S. et al., 2022. Overview of the Jack Rabbit II (JR II) field experiments and summary of the methods used in the dispersion model comparisons. *Atmospheric Environment*, January, Volume 269, p. 118783.

Kamotani, Y. & Greber, I., 1971. *Experiments on a Turbulent Jet in a Cross Flow*, s.l.: s.n.

Kamotani, Y. & Greber, I., 1972. Experiments on a Turbulent Jet in a Cross Flow. *AIAA Journal*, 11, Volume 10, p. 1425–1429.

Linden, P. F. & Simpson, J. E., 1988. Modulated mixing and frontogenesis in shallow seas and estuaries. *Continental Shelf Research*, October, Volume 8, p. 1107–1127.

Mahesh, K., 2013. The Interaction of Jets with Crossflow. *Annual Review of Fluid Mechanics*, 1, Volume 45, p. 379–407.

Mazzola, T. et al., 2021. Results of comparisons of the predictions of 17 dense gas dispersion models with observations from the Jack Rabbit II chlorine field experiment. *Atmospheric Environment*, August.p. 117887.

McQuaid, J. & Roebuck, B., 1985. *Large Scale Field Trials on Dense Vapour Dispersion. Final Report to Sponsors on the Heavy Gas Dispersion Reials at Thorney Island 1982-1984*, s.l.: s.n.

Morton, B. R., Taylor, G. I. & Turner, J. S., 1956. Turbulent gravitational convection from maintained and instantaneous sources. *Proceedings of the Royal Society of London. Series A. Mathematical and Physical Sciences*, Volume 234, p. 1–23.

Muppidi, S. & Mahesh, K., 2008. Direct numerical simulation of passive scalar transport in transverse jets. *Journal of Fluid Mechanics*, Volume 598, p. 335.

Ooms, G., 1972. A new method for the calculation of the plume path of gases emitted by a stack. *Atmospheric Environment (1967)*, 12, Volume 6, p. 899–909.

Petersen, R. L. & Ratcliff, 1989. *Effect of homogeneous and heterogeneous surfaceroughness on HTAG dispersion*, Ft. Collins: s.n.

Post, L. & others, 1994. HGSYSTEM 3.0 technical reference manual. *Report No. TNER*, Volume 94.

Pratte, B. D. & Baines, W. D., 1967. Profiles of the round turbulent jet in a cross flow. *Journal of the Hydraulics Division*, Volume 93, p. 53–64.

Quillatre, P., 2017. *Relevance of the current modelling methods for the prediction of LNG vapour dispersion and development to be carried on.* s.l., s.n.

Schatzmann, M., Snyder, W. H. & Lawson, R. E., 1993. Experiments with heavy gas jets in laminar and turbulent cross-flows. *Atmospheric Environment. Part A. General Topics*, May, Volume 27, p. 1105–1116.

Vidali, C. et al., 2019. Atmospheric dispersion of heavy gas and passive scalar emission from elevated source.

Witcofski, R. & Chirivella, J., 1984. Experimental and analytical analyses of the mechanisms governing the dispersion of flammable clouds formed by liquid hydrogen spills{\ding{73}}. *International Journal of Hydrogen Energy,* Volume 9, p. 425–435.

Witlox, H. W. M. et al., 2018. Verification and validation of Phast consequence models for accidental releases of toxic or flammable chemicals to the atmosphere. *Journal of Loss Prevention in the Process Industries,* September, Volume 55, p. 457–470.

Witlox, H. W. M. & Holt, A., 1999. *A unified model for jet, heavy and passive dispersion including droplet rainout and re-evaporation.* s.l., s.n.

Yuan, L. L. & Street, R. L., 1998. Trajectory and entrainment of a round jet in crossflow. *Physics of Fluids,* 9, Volume 10, p. 2323–2335.